Slow dynamics in semiconductor multi-longitudinal-mode laser transients governed by a master mode

N. Dokhane,[1] G. P. Puccioni,[2] and G. L. Lippi[3,4,*]

[1]*Department of Physics, Faculty of Science, University of M'Hamed Bougara, Boumerdes, Algeria*

[2]*Istituto dei Sistemi Complessi, CNR, Via Madonna del Piano 10, I-50019 Sesto Fiorentino, Italy*

[3]*Institut Non Linéaire de Nice, Université de Nice Sophia Antipolis, Valbonne, France*

[4]*CNRS, UMR 7335, 1361 Route des Lucioles, F-06560 Valbonne, France*

(Received 20 February 2012; published 16 April 2012)

We examine the response to the sudden switch of the pump parameter in a multimode semiconductor laser with intensity coupling on a model whose validity has been successfully compared to experimental results. We find the existence of a very slow modal evolution governed by a *master mode*, which reaches its steady state on a time scale that is a couple of orders of magnitude longer than that of the total intensity. The practical consequences for applications are examined, such as the temporal evolution of the spectral width of the laser emission and the time at which its steady state is attained. Issues related to modeling choices, such as the number of modes and their placement with respect to line center, are discussed.

DOI: 10.1103/PhysRevA.85.043823 PACS number(s): 42.55.Px, 42.60.Mi, 05.45.−a

I. INTRODUCTION

When turning on a laser, the typical variable which is experimentally, and most easily, monitored is the total output intensity. While on the practical side this choice is a sensible one, earlier results have shown, both theoretically and experimentally, that multi-longitudinal-mode regimes exist where an underlying, long-term, residual intermodal dynamics may exist [1–6]. In such a case, the information gathered through the total intensity is incomplete and may hide not only important aspects of the physics of the problem but also some technologically important side effects. Semiconductor lasers may also hide their modal dynamics under a constant or nearly constant laser intensity, the so-called *antiphase dynamics regime*, where the individual modes oscillate in such a way as to share the available gain in a cooperative fashion [7–9], while slow, dynamical modal features may remain hidden in the modeling of strongly multimode systems [10–12].

In order to investigate the switch-on transient in a semiconductor laser, we have studied a multi-longitudinal mode, with intensity coupling, whose predictions in the transient regime have been compared to experimental results [13]. In this investigation we consider the crossing of the laser threshold in response to a sudden switch in the pump. The focus of our attention is the evolution of the transient from the moment when the control parameter (the pump in our case) is suddenly increased to the time when the system has attained its final steady state. The problem is well posed for semiconductor lasers because there exist regimes of stable multimode operation above threshold, contrary to what happens for classic homogeneously broadened systems [14]. The interest in such a question is mainly fundamental: understanding the intermode dynamics which underlies the global temporal laser behavior usually monitored through the total laser output. We remark that these results may apply to other class B lasers [15] since the findings do not depend on the specifics of the model, but rather on the generic structure of the coupling. Finally, our results may also benefit applications in situations where the temporal evolution of the spectral content of the laser output is crucial (e.g., in the spectral content of short temporal pulses).

Section II briefly presents the model under study with some discussion about the physics of the system and the choices we have made for its numerical integration; the definitions for the various parameters and their values can be found in the Appendix. The numerical results obtained by the straightforward integration of the model when switching the pump parameter from below to above threshold are discussed in Sec. III. An analytical approach is developed in Sec. IV, where we interpret, on the basis of the model's structure, the numerical findings. The slow energy redistribution among modes is discussed in Sec. IV A, while a simplified, toy model is used in Sec. IV B to explain the global behavior of the modal variables in the slow evolution phase. Section IV C highlights the role of the master mode in the dynamics. Issues related to the choice of mode positioning relative to the gain peak are examined in Sec, V. A summary of the paper and some conclusions are offered in Sec. VI.

II. MODEL

We study a model for a multi-longitudinal-mode semiconductor laser whose parameter values have been determined to match experimental results [13]. As in all rate equations models, the dynamics here are described in terms of time-dependent ordinary differential equations (ODEs) for each modal intensity. All interference phenomena are neglected since the intermode spacing (typically $\Delta\nu \approx 1.5 \times 10^{11}$Hz) is small enough compared to the laser's internal rates (relaxation oscillation frequency $<10^{10}$ Hz) to average out the fast oscillations [16]. A thorough discussion of the conditions under which the phase dynamics (intermode beating) can be neglected can be found in [17].

Coupling between the different laser modes occurs through the population inversion, which acts as a global energy

*gian-luca.lippi@inln.cnrs.fr

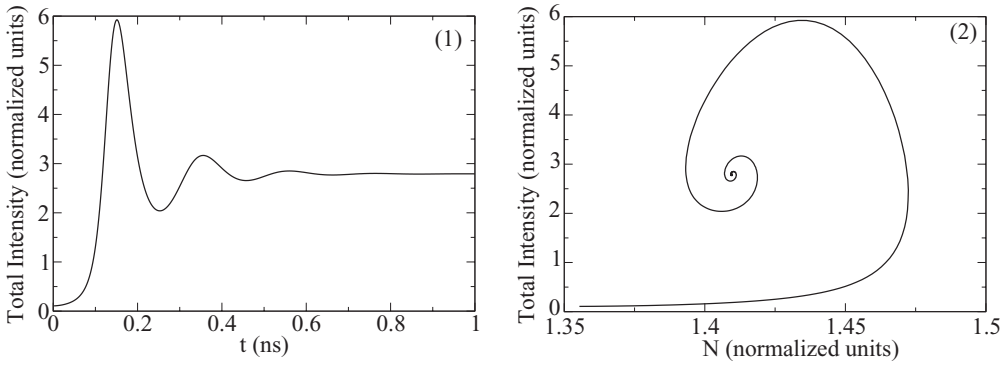

FIG. 1. Time evolution of the total laser intensity [panel (1)] following a sudden switch-on of the injected current (pump rate) in the form of a Heaviside function. Phase-space representation [panel (2)] of the switch picturing the total intensity I_t as a function of the carrier number N. Initial current value $J_i = 15.5$ mA; final current value $J_f = 37.5$ mA. The threshold current for this laser is $J_{\text{th}} = 17.5$ mA. The number of modes used for the integration is 113. All other parameters are as in Table III. All parameter values are kept constant throughout this paper, unless otherwise explicitly noted. The delay at turn-on is approximately $t_d \approx 0.1$ ns, while the steady state is attained at $\bar{t} \simeq 0.7$ ns. Here and in all subsequent figures (unless otherwise noted) the total intensity I_t is divided by 10^5, and the number of carriers N is divided by 10^8.

reservoir for them all. The model equations are [13]

$$\frac{dI_j(t)}{dt} = \left[\Gamma G_j(N) - \frac{1}{\tau_p}\right] I_j + \beta_j B N(N + P_0), \quad \text{(1a)}$$

$$\frac{dN(t)}{dt} = \frac{J}{q} - R(N) - \sum_j \Gamma G_j(N) I_j, \quad \text{(1b)}$$

where $I_j(t)$ is the intensity of each longitudinal mode of the electromagnetic (e.m.) field ($1 \leqslant j \leqslant M$), $N(t)$ is the number of carriers as a function of time, Γ is the optical confinement factor, $G_j(N)$ is the optical gain for the jth lasing mode (function of carrier number and wavelength), τ_p is the photon lifetime in the cavity, β_j is the fraction of spontaneous emission coupled in the jth lasing mode, B is the band-to-band recombination constant, P_0 is the intrinsic hole number in the absence of injected current, J is the current injected into the active region, q is the electron charge, and $R(N)$ is the incoherent recombination term (including radiative and nonradiative recombination), which represents the global loss terms for the carrier number (i.e., the population inversion in the usual laser language). All definitions for the functions and all values for the physical parameters are given in the Appendix.

The term in brackets in Eq. (1a) represents the global gain for each laser mode, with the first part accounting for the actual source terms and the second for the out-coupling losses. The last term in the equation takes into account the average contribution of the spontaneous emission to each lasing mode. In the equation for the number of carriers in the conduction band, the first term represents the pump. The second term in Eq. (1b) describes the losses for the carrier density due to different processes, while the last term accounts for the (global) reduction in population due to the energy transferred to the different intensity modes. This last term is the source of coupling among all modes.

In the numerical simulations, we have included 113 modes to cover approximately 1.5 times the FWHM of the gain curve (cf. Appendix for additional details). Only a subset of these modes actually lases at steady state, but their large number ensures that the *slow dynamics* is initiated with reliable, simulation-independent *initial conditions* for the lasing modes.

III. THRESHOLD CROSSING

We analyze the laser's behavior when it crosses the threshold in the total intensity [the variable that is normally measured; Fig. 1, panel(1)] and in the modal intensities. The total intensity shows the characteristic turn-on with intensity overshoot and damped oscillations which disappear at $\bar{t} \simeq 0.7$ ns. Figure 1, panel (2), shows the corresponding phase-space portrait, with the typical spiralling relaxation toward the stable focus [19] (lasing solution).

Figure 2 shows a detail of Fig. 1, panel (2), where crossing trajectories become apparent. They are due to the two-dimensional (2-D) projection onto the (N, I_t) plane of the 114-D space and imply the existence of an underlying dynamics hidden under the apparent steady state of Fig. 1. Accompanying tiny variations in I_t are present, even though they are not clearly visible in Fig. 2.

Figure 3 shows the long-time evolution of selected modes: central [$j = 57$, curve (d)], first side mode [$j = 56$, curve (c)], and two additional side modes close to line center [$j = 54$,

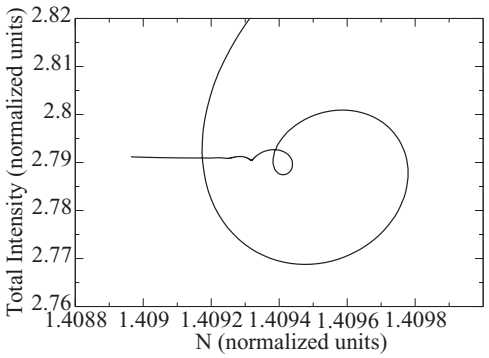

FIG. 2. Detail of the phase space of Fig. 1, panel (2), suggesting the presence of a residual evolution arising from the interplay among the different lasing modes.

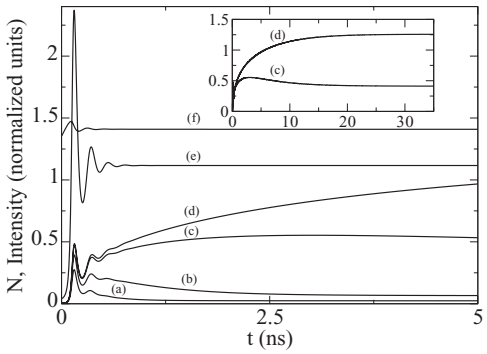

FIG. 3. Total intensity [curve (e)] and carrier number [curve (f)] as a function of time. The other curves show the individual mode intensities for the central mode [$j = 57$, curve (d)] and side modes close to line center (blue side): $j = 56$ [curve (c)], $j = 54$ [curve (b)], and $j = 52$ [curve (a)]. The symmetric modes, relative to the central one, are not shown but are identical. Notice that in the first phases of the transient (peak) curves (c) and (d) are superposed: they separate only at the second oscillation. For graphical purposes the curves are scaled as follows: here I_t is divided by 2.5×10^5, and the individual mode intensities are divided by 10^5 (here and in all subsequent figures, unless otherwise noted). The inset shows the long-time evolution of the central mode (d) and of the first side mode (c): steady state is attained by the central mode at $t \approx 35$ ns.

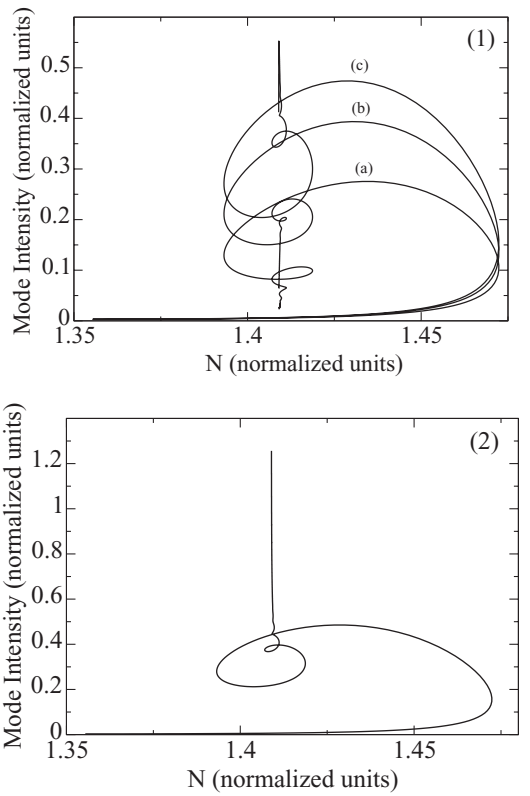

FIG. 4. Phase-space portrait of the transient displayed in Fig. 3. Panel (1) shows the evolution of the side modes: $j = 56$ [curve (c)], $j = 54$ [curve (b)], and $j = 52$ [curve (a)]. Panel (2) gives the evolution of the central mode. Notice the different vertical scales. See the caption of Fig. 3 for details.

curve (b), and $j = 52$, curve (a)]; for comparison the (rescaled) carrier number N [curve (f)] and total intensity I_t [curve (g)] are displayed. The inset shows the long-time evolution (over 35 ns) of the central mode and of the first side mode. While the total intensity and the population inversion reach steady state at time $\bar{t}$, the individual modes continue their evolution on a much longer time scale. The central mode, curve (d), continues to grow and arrives at its final value only for $t_{c,ss} \approx 35\text{ns} \approx 50\bar{t}$ (inset). The next side mode (and its symmetric around line center) reaches its steady state somewhat faster (inset) by first overshooting the final value and then relaxing toward it. Moving away from line center, the modal relaxation time decreases, together with the steady-state output power.

Finally, Fig. 4 shows the phase-space portrait for the central mode [Fig. 4, panel (2)] and for the side modes [Fig. 4, panel (1)]: the *usual* dynamics of single-mode lasers (a spiral around the fixed point; cf., e.g., Fig. 1 in [20]) is complemented by a sizable evolution in the modal intensities (occupying two-thirds of the amplitude interval for the central mode) at constant (or nearly constant) N. Only the central mode attains a steady-state intensity that monotonically grows: All side modes possess a transient peak intensity larger (or even much larger) than their corresponding steady states. The first side mode ($j = 56$ and its symmetric, $j = 58$) reaches its highest intensity on the slow evolution [sharp peak in Fig. 4, curve (c), to be matched to the peak in the inset of Fig. 3, curve (c)].

In order to avoid lengthy numerical integrations, approximate, but rather accurate, analytical modal expressions were obtained for similar semiconductor laser models [21]. Here, instead, we are interested in understanding the physical origin of the slow dynamics and its practical implications in modeling and numerical accuracy. Thus, we will employ different tools, including some analytical considerations, to attain our goal.

IV. ANALYSIS

The analysis of these numerical observations proceeds as follows. In Sec. IV A we remark on the possible existence of a *partial steady state* for the total laser intensity and for the carrier density and on the constraints which its existence imposes on the ensuing modal dynamics. Section IV B highlights, with the help of a strongly simplified analysis, the crucial role of the modal gain vs losses and shows the existence of a *master mode*. The influence of the latter on the slow laser dynamics are discussed in Sec. IV C.

A. Slow dynamics

The numerical results convincingly suggest that one should analyze the dynamics by introducing one *global* variable in Eqs. (1): the total intensity I_t. The laser description is therefore based on I_t and N as global variables and $M - 1$ individual modal intensities:

$$\frac{dI_t}{dt} = \sum_j^M \Gamma G_j(N) I_j - \frac{1}{\tau_p} I_t + \beta_t B N (N + P_0), \quad (2a)$$

$$\frac{dN(t)}{dt} = \frac{J}{q} - R(N) - \sum_j^M \Gamma G_j(N) I_j, \quad (2b)$$

$$\frac{dI_j(t)}{dt} = \left[\Gamma G_j(N) - \frac{1}{\tau_p}\right] I_j + \beta_j B N (N + P_0), \quad 1 \leqslant j \leqslant M - 1, \quad (2c)$$

where we have defined the contribution of the spontaneous emission to all modes $\beta_t = \sum_j^M \beta_j$.

Inspection of Eqs. (2a) and (2b) for the *global* variables (N, I_t) shows a high degree of symmetry and a strong resemblance to an equivalent model for a single-longitudinal-mode laser [22]. The coupling between these two variables is entirely symmetric $[\sum_j^M \Gamma G_j(N) I_j]$, as for the single-mode laser, hence the (N, I_t) dynamics of Fig. 1, reminiscent of a single-mode laser, where the competition between the (slow) energy reservoir (population inversion) and the fast relaxing electromagnetic field (intensity) produce an oscillatory approach toward the lasing state.

A more formal analysis is based on the steady states, denoted by the overline and obtained from Eqs. (2a) and (2b):

$$\sum_j^M \Gamma G_j(\overline{N}) I_j = \frac{1}{\tau_p} \overline{I}_t - \beta_t B \overline{N}(\overline{N} + P_0), \tag{3a}$$

$$\sum_j^M \Gamma G_j(\overline{N}) I_j = \frac{J}{q} - R(\overline{N}). \tag{3b}$$

These two conditions define $\overline{I}_t$ and $\overline{N}$. Combining Eqs. (3a) and (3b), we find

$$\overline{I}_t = \left[\frac{J}{q} - R(\overline{N}) + \beta_t B \overline{N}(\overline{N} + P_0) \right] \tau_p, \tag{4}$$

independently of the individual mode intensity values. The expression for $\overline{N}$ is given in implicit form by Eq. (3b). In spite of the fact that its explicit expression involves the sum over all individual intensity modes, each multiplied by its gain function $G_j(\overline{N})$ calculated at $N = \overline{N}$, it is certain that the expression is satisfied at steady state and that a unique value exists. Indeed, although the individual mode intensities come into play, $G_j(\overline{N})$ represents a set of constants once $N = \overline{N}$. In other words, starting from time $t = \bar{t}$ [at which $I_t(\bar{t}) = \overline{I}_t$ and $N(\bar{t}) = \overline{N}$], $\overline{N}$ remains constant [since $\frac{dN}{dt}_{t=\bar{t}} = 0 \Rightarrow N(t > \bar{t}) = \overline{N}$] [23].The residual modal dynamics must therefore comply with the constraint that the left-hand side (lhs) of Eq. (3b) remain constant [since the right-hand side (rhs) will not change in time].

More formally, the following constraints hold:

$$\sum_j I_j = \overline{I}_t = K_1, \tag{5a}$$

$$\sum_j \Gamma G_j(\overline{N}) I_j = \frac{J}{q} - R(\overline{N}) = K_2, \tag{5b}$$

where K_1 and K_2 are two constants which characterize the laser operation for each set of parameter values.

The fact that the sum on the lhs of Eq. (5b) is a constant, K_2, does not exclude a residual time evolution among the modes, which are numerous enough to arrange for that. This becomes apparent by rewriting the evolution equation for the individual modes after the equilibrium condition for the total intensity and the population variable have been attained (hence, with $N = \overline{N}$ everywhere):

$$\frac{dI_j}{dt} = \left[\Gamma G_j(\overline{N}) - \frac{1}{\tau_p} \right] I_j + \beta_j B \overline{N}(\overline{N} + P_0). \tag{6}$$

TABLE I. Numerical values for the two terms which compose the rhs of the evolution equation for the modal intensity, Eq. (6), listed for selected modes after steady state has been attained by the *global variables*. $\mathcal{A}$ and $\mathcal{B}$ represent $\Gamma G_j(\overline{N}) - (1/\tau_p)$ and $\beta_j B \overline{N}(\overline{N} + P_0)$, respectively. The values are estimated at $t = 35$ ns to eliminate any the residual dynamics on N.

Mode j	λ_j (μm)	$\mathcal{A}$ (s^{-1})	$\mathcal{B}$ (s^{-1})
57	1.3	-8.44×10^7	1.0623×10^{13}
56	1.2994	-2.58×10^8	1.0621×10^{13}
54	1.29819	-1.65×10^9	1.0601×10^{13}
52	1.29698	-4.43×10^9	1.0563×10^{13}
50	1.29578	-8.59×10^9	1.0506×10^{13}
40	1.28974	-5.03×10^{10}	9.9673×10^{12}
30	1.2837	-1.27×10^{11}	9.1109×10^{12}
20	1.27767	-2.38×10^{11}	8.0987×10^{12}
10	1.27163	-3.84×10^{11}	7.0681×10^{12}

Three remarks are necessary here.

(1) The term in square bracket on the rhs of Eq. (6) (coefficient of I_j) plays the role of an *effective relaxation constant* for each field intensity, given by the difference between the individual gain term for the individual mode and the cavity losses (equal for all modes). The second term in the equation is a constant in time (different for each mode via β_j) now that the $N = \overline{N}$ state has been attained.

(2) The different values of $G_j(\overline{N})$ imply that the *effective relaxation constant* is different for each mode; hence, those modes that have larger coefficients in front of I_j will evolve more rapidly, while the long-term dynamics will be governed by the slower modes (cf. Table I for numerical values).

(3) Since the steady-state values $N = \overline{N}$ and $I_t = \overline{I}_t$ have been attained, the evolution equations for the individual modes, Eq. (6), are now almost decoupled: they only need to obey to the constraints, Eqs. (5), for all $t > \bar{t}$ ($\bar{t}$ being the time at which the global variables attain their equilibrium condition).

Notice that there is no contradiction between the global constraint $\sum_j^M I_j = \overline{I}_t = K_1$ and the fact that the time scales for the evolution may be different. Indeed, the evolution for each mode is the result of the difference between $\overline{I}_t$ and all other modes, thus allowing for the appearance of different time scales in the mode combination.

Table I clearly shows that the spontaneous emission contribution $\mathcal{B}$ varies very little between the central and the side modes ($\mathcal{B}_{57} \approx 1.5 \times \mathcal{B}_{10}$). Instead, the effective relaxation constant $\mathcal{A}$ (Table I) changes by more than four orders of magnitude and dominates the dynamics. The ratio $\mathcal{A}(j = 57) \approx 2 \times 10^{-2} \mathcal{A}(j = 52)$ suggests that mode $j = 52$ should attain its steady state in a time approximately 50 times shorter than the central mode. Inspection of Fig. 3 qualitatively confirms this result, thus validating our simple interpretation of the dynamics in terms of (nearly) decoupled groups of variables: (N, I_t) on the one hand and I_j $(j = 1 \ldots M - 1)$ on the other.

From the data in Table I we can also draw additional information about the long-term dynamics of the individual

modes. The evolution of each mode is determined by Eq. (6), whose rhs reads $\mathcal{A}_j I_J + \mathcal{B}_j$. Reading the intensity values for modes with $j = 57$, $j = 56$, and $j = 54$ off Fig. 3 at the end of the transient for the total intensity I_t (and the population N), we estimate the rhs to give $\frac{dI_{57}}{dt}|_{t\approx 0.7ns} \approx 7 \times 10^{12}$ [$I_{57}(t \approx 0.7\text{ns}) \approx 4 \times 10^4$], $\frac{dI_{56}}{dt}|_{t\approx 0.7ns} \approx 3 \times 10^{11}$ [$I_{56}(t \approx 0.7\text{ns}) \approx 4 \times 10^4$], and $\frac{dI_{54}}{dt}|_{t\approx 0.7ns} \approx -2 \times 10^{13}$ [$I_{54}(t \approx 0.7\text{ns}) \approx 2 \times 10^4$]. We see immediately that modes $j = 57$ and $j = 56$ must grow, while all other modes should decay from the value that they have reached at the end of the transient for the global variables. This prediction is confirmed by the results displayed in Fig. 3. Note that the values for the constants given in Table I apply since starting from the end of the transient for the global variables coefficients $\mathcal{A}$ and $\mathcal{B}$ no longer depend on time. We can further remark that the reversal in the growth of mode $j = 56$ can also be interpreted on the basis of the effective relaxation constant since during the slow evolution, due to the interplay with all other modes, this mode acquires an intensity value which inverts the sign of its rhs in Eq. (6): $\frac{dI_{56}}{dt}|_{t\approx 3ns} \approx -4 \times 10^{12}$ [$I_{56}(t \approx 3\,\text{ns}) \approx 5.5 \times 10^4$].

In the following section we show that the time scale over which the steady state for *all* modes is attained (the true steady state for the system) is determined by the mode with the highest gain. We will see that the initial conditions play only a minor role (determining the quantitative aspects of the dynamics) and that the contribution of the spontaneous emission [the last term in Eq. (6)] can be neglected.

B. Role of the physical constants

Since we analyze the dynamics after the *global* variables have attained their steady-state condition ($t > \bar{t} \simeq 0.7$ ns) and the constraint over the sum of all the modes holds, all expressions involving these variables can be taken to be constants. Thus the following simplified analysis holds and pertinently highlights the influence of the various elements on the slow modal evolution. For the purpose of illustration (Fig. 5), we use a number of modes much smaller than in the full simulations. Our arguments are, however, independent of this choice.

Rewriting Eq. (6) as

$$\frac{dI_j}{dt'} = -\mathsf{a}_j I_j + \mathsf{b}_j, \qquad \mathsf{a}_j, \mathsf{b}_j > 0, \tag{7}$$

[t' being a time variable different from that of Eqs. (1)] and integrating it formally [24], we obtain

$$I_j(t') = \mathsf{C}_j e^{-\mathsf{a}_j t'} + \frac{\mathsf{b}_j}{\mathsf{a}_j}. \tag{8}$$

The constraint on the total laser intensity still holds, even though it does not appear explicitly. The sign of C_j, a constant which functionally depends on the initial condition $I_j(\bar{t})$, determines whether the further evolution of the mode consists of a decrease ($\mathsf{C}_j > 0$) or an increase ($\mathsf{C}_j < 0$) of each I_j. The explicit form of the C_j's can easily be written as a function of the initial condition for each mode I_{j0}:

$$\mathsf{C}_j = \left(I_{j0} - \frac{\mathsf{b}_j}{\mathsf{a}_j}\right), \tag{9}$$

where we have taken $t' = t - \bar{t}$, so that our initial condition is specified at $t' = 0$. Thus the explicit form of Eq. (8) becomes

$$I_j(t') = \frac{\mathsf{b}_j}{\mathsf{a}_j}\left[1 + \frac{\mathsf{a}_j}{\mathsf{b}_j}\left(I_{j0} - \frac{\mathsf{b}_j}{\mathsf{a}_j}\right) e^{-\mathsf{a}_j t'}\right], \tag{10}$$

where I_{j0} is the intensity of each mode when the *global* variables attain steady state (at $t' = 0$). It is easy to see that neither the value of I_{j0} nor that of b_j plays a substantial role in the subsequent dynamics. Indeed, if we consider two constants I_0 and b equal for all modes and write therefore the solution, Eq. (10), as

$$I_j(t') = \frac{\mathsf{b}}{\mathsf{a}_j}\left[1 + \frac{\mathsf{a}_j}{\mathsf{b}}\left(I_0 - \frac{\mathsf{b}}{\mathsf{a}_j}\right) e^{-\mathsf{a}_j t'}\right], \tag{11}$$

we are still able to reproduce the overall slow dynamics of the various laser modes by appropriately choosing the a_j's.

The numerical integration of the two sets of equations, Eqs. (10) and (11), shows that the difference in the evolution is only quantitative [cf. Figs. 5, panels (1) and (2), respectively]. Hence, we conclude that the slow dynamics result from the *equivalent relaxation constants* a_j for each mode and depend only in a minor fashion on the values actually taken by each mode at $t = \bar{t}$ (the end of the transient for the global variables) or on the fraction of spontaneous emission injected in each mode (represented by b_j). Instead, through the factor $\mathsf{C}_j(I_{j0} = I_0)$, the a_j's determine the exponential growth and decay (small and large a_j, thus $\mathsf{C}_j \lessgtr 0$) to a finite and zero value for the corresponding mode, respectively. Inspection of Eq. (11) shows that the smaller a_j is, the larger the asymptotic value of $I_j(t' \to \infty) = \frac{\mathsf{b}}{\mathsf{a}_j}$ is.

In our semiconductor laser model, a_j corresponds to the square bracket in Eq. (1a) and thus to the loss-gain balance. As is the case in all dynamical systems [25], the slowest growth will be that of the mode with the (negative) value of a_j closest to zero: the mode with the largest gain. Only after this mode has reached its steady state will the dynamics be completed.

C. Master mode

The previous simplified analysis clearly shows how the mode with the highest gain possesses the slowest relaxation constant and is therefore the last to attain equilibrium. This mode can be considered to be the *master mode* which *enslaves* [26] the other modes, as is best seen by the following considerations. The constraints, Eqs. (5a) and (5b), imply that at time $t > \bar{t}$ the individual modes must maintain the total output power constant. The slow growth of the master mode forces the other lateral modes to compensate for its sluggishness. During the transient ($t \leqslant \bar{t}$), the modes farthest away from line center acquire values which are well beyond their steady states and then fade away. However, even during the slow dynamics the lateral modes are not the *actors* of the dynamics, but only the *followers*. Indeed, the first two side modes ($j = 56$ and, symmetrically, $j = 58$) are initially forced to grow *beyond* their steady-state value [Fig. 4, panel (1), curve (c)] toward which they eventually decay away. This nonmonotonic behavior, which characterizes all the enslaved modes, is the proof that only one master mode exists and that it alone determines all the dynamics.

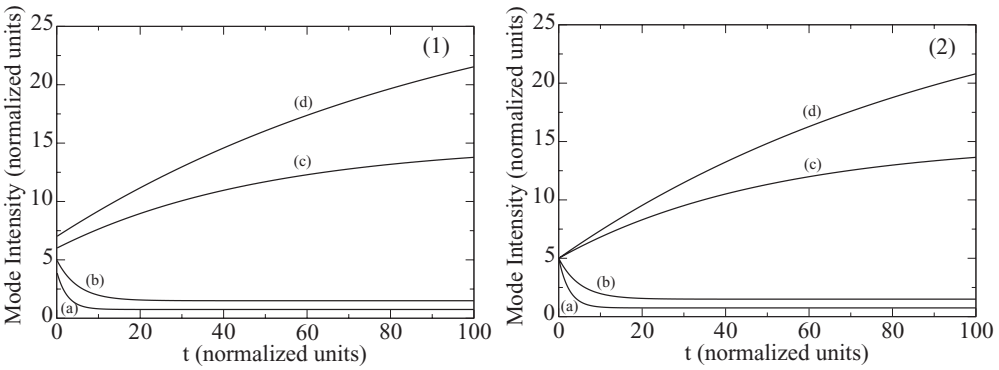

FIG. 5. Illustration of the evolution of a mode described by the simplified approach of Eq. (10) [panel (1)] with different *initial values* for the modal intensity I_{j0} at $t' = 0$ and for the b_j's. Panel (2) shows the equivalent calculation based on Eq. (11), obtained with only one value for I_0 and b. Aside from a small quantitative difference, the evolution shown in panels (1) and (2) is qualitatively the same. Panel (1) curves are (a) $I_{0a} = 4$, $\frac{\mathsf{a}_a}{\mathsf{b}_a} = 1.33$; (b) $I_{0b} = 5$, $\frac{\mathsf{a}_b}{\mathsf{b}_b} = 0.667$; (c) $I_{0c} = 6$, $\frac{\mathsf{a}_c}{\mathsf{b}_c} = 6.67 \times 10^{-2}$; (d) $I_{0d} = 7$, $\frac{\mathsf{a}_d}{\mathsf{b}_d} = 3.33 \times 10^{-2}$. Panel (2) curves are $I_0 = 5$, $\mathsf{b} = 0.3$, and (a) $\mathsf{a}_a = 0.4$; (b) $\mathsf{a}_b = 0.2$; (c) $\mathsf{a}_c = 0.02$; (d) $\mathsf{a}_d = 0.01$. The values for the coefficients are chosen in such a way as to obtain a good qualitative illustration of the actual evolution of the different laser modes.

V. EVEN VERSUS ODD NUMBER OF MODES

The simulations discussed so far are performed with an odd number of modes, with the central one placed exactly at the peak of the gain line. It is crucial to know whether, and how, a different choice may influence the numerical results. Indeed, the results should be invariant with respect to this choice; otherwise, the reliability of the whole approach is called into question. More interestingly, in experimental situations there is no guarantee that a centered mode exists on the gain line: first, because the position of each mode depends on the cavity length, which varies as a function of numerous parameters (construction, temperature, saturation, etc.), second because it is well known that in semiconductor lasers the gain line is subject to a nonnegligible frequency shift (not included in the present model), and third because the real line shape of a semiconductor laser is asymmetric [27–29] and therefore a *line center* is only ill defined.

The maximum deviation from the computation with an odd number of modes, exactly centered at the gain peak, is obtained by choosing an even number of modes, placed symmetrically with respect to line center. All other configurations are intermediate between these two and will be covered by the two extreme choices that we examine.

Simulation of the same equations with $M = 112$ modes provides predictions for the global variables, which are indistinguishable from those obtained with $M = 113$ modes, thus confirming the validity of the approach. Problems, however, are detected by looking at the individual mode evolution.

Figure 6 compares the long-term evolution of the central mode for $M = 113$ ($j = 57$) [curve (a)] and for $M = 112$ ($j = 56$) [curve (c)]. Aside from the difference in height in the two curves (i.e., their relative intensity), a trivial fact directly related to the difference in energy distribution, we notice that the time to reach the asymptotic value differs. The explanation for the faster convergence lies in the fact that the *central mode*, off line center, has a more negative (larger in absolute value) *effective relaxation rate* (Table II). Comparing the numerical derivatives for the central mode I_c (corresponding to $j = 57$ for $M = 113$ modes and to $j = 56$ for $M = 112$ modes) directly on the integration, we find that $\frac{dI_c}{dt}|_{M=112}(t = 14\ \text{ns}) \approx \frac{dI_c}{dt}|_{M=113}(t = 27\ \text{ns})$: convergence appears to be approximately twice as fast when using an even number of modes symmetrically placed with respect to line center.

Figure 6 also compares two side modes. For both modal placements the first side modes display an initial overshoot, with exponential relaxation toward their respective steady states. The difference in amplitude [curves (b) and (d)] is, not surprisingly, due to their different position underneath the gain line and to the energy distribution among modes for even vs odd number of modes, but the relaxation time is, again and for the same reasons, shorter for an even number of modes. Thus, we conclude there is again "one" master mode (doubled, due to the symmetric choice in modal placement) which dominates

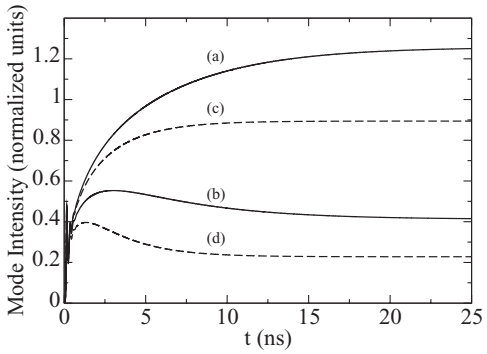

FIG. 6. Comparison of the long-time evolution for odd and even numbers of modes in the simulation. Curve (a) is the center mode ($j = 57$) and curve (b) is the first side mode ($j = 56$) for $M = 113$ modes. Curve (c) is the center mode ($j = 56$) and curve (d) is first side mode ($j = 55$) for $M = 112$ modes. The difference in height between the modes at line center is explained by the fact that for even M, the intensity is distributed between the two symmetric modes, while for odd M more of it is concentrated in the central mode. Overall, the intensity distribution is somewhat different. Conditions for integration are the same as for an odd number of modes (save for the value of M). For graphical purposes, the modal intensities are still divided by 10^5.

TABLE II. $M = 112$ modes. Numerical values for the two terms which compose the rhs of the evolution equation for the modal intensity, Eq. (6), listed for selected modes after steady state has been attained by the *global variables*. $\mathcal{A}$ and $\mathcal{B}$ represent $\Gamma G_j(\overline{N}) - (1/\tau_p)$ and $\beta_j B\overline{N}(\overline{N} + P_0)$, respectively. The values are taken at $t = 35$ ns to ensure convergence. Notice the sizable change in the values of the coefficients of I_j in Eq. (1a) between Table I and the present one due to the change in wavelength and thus in the position relative to line center (peak wavelength $\lambda_p = 1.3$ μm). The relative change for the central mode is approximately 40%. The spontaneous emission contribution remains, instead, practically unchanged.

Mode j	λ_i (μm)	$\mathcal{A}$ (s^{-1})	$\mathcal{B}$ (s^{-1})
56	1.2997	-1.16×10^8	6.610×10^8
54	1.29849	-1.16×10^9	6.604×10^8
52	1.29728	-3.59×10^9	6.586×10^8
50	1.29608	-7.41×10^9	6.556×10^8
40	1.29004	-4.73×10^{10}	6.246×10^8
30	1.28401	-1.22×10^{11}	5.728×10^8
20	1.27797	-2.31×10^{11}	5.104×10^8
10	1.27193	-3.76×10^{11}	4.461×10^8

the dynamics, but its numerical convergence is now twice as fast, speeding up also the convergence toward the complete steady state.

When looking at the evolution of the emitted spectrum (i.e., intensity distribution over the different modes) the placement of the modes under the gain line acquires additional importance. On the one hand, the later convergence of the central mode, when perfectly centered, delays the spectrum from attaining its asymptotic form. On the other hand, we see that the predicted spectral width strongly depends on this choice. Indeed, by defining the full spectral width W_{20}^{FS} as the frequency interval (interpolated between the two closest modes) in which the intensity passes the -20 dB mark relative to the total intensity, one sees from Fig. 7 that $\frac{W_{20}^{\mathrm{FS}}(113\ \mathrm{modes}) - W_{20}^{\mathrm{FS}}(112\ \mathrm{modes})}{W_{20}^{\mathrm{FS}}(112\ \mathrm{modes})} \approx 1.6$.

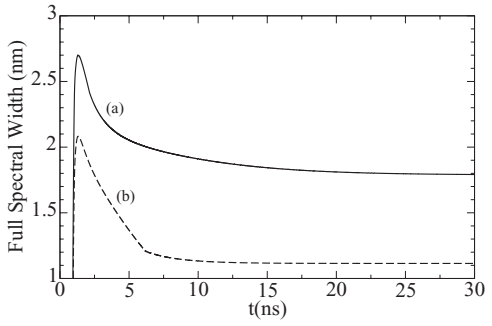

FIG. 7. Spectral footprint of the laser evolution during transient. Curves (a) and (b) show the full spectral width, in nanometers, at -20 dB (W_{20}^{FS}) calculated for 113 modes (solid line) and for 112 modes (dashed line). The level is calculated relative to the instantaneous total intensity. The *late start* of the W_{20}^{FS} curves indicates that the intensity is spread on a large number of modes in the fast part of the transient, a fact that also is reflected in the wider spectral width at times $1 < t < 5$ ns. Notice that the final value of the spectral width differs considerably (by approximately 1.6 times) depending on the modeling choice.

We can therefore conclude that depending on the choice of modal arrangement (symmetry with respect to the peak of the gain line and distance between modal wavelength and peak wavelength), (a) the global variables are not affected, (b) the intensity distribution among modes changes rather substantially, (c) the frequency spectrum is substantially different when looking at the W_{20}^{FS}, and (d) the time necessary to attain the asymptotic spectral distribution of intensity changes very substantially. The latter remark can be particularly problematic when one tries to obtain information about the time-resolved spectral content. Indeed, on the one hand, it is known that for *long* semiconductor lasers the time necessary to attain the asymptotic spectrum is long compared to the total intensity transient [21]. On the other hand, the great variations (a factor of 2) in the time necessary to reach spectral equilibrium depending on the simulation choices should make one wonder about the meaningfulness of the predictions. Further work, with close comparison to experimental results, is necessary to answer this question.

In practice, semiconductor lasers are intrinsically very sensitive to temperature and thus to power level. Carrier density can also influence the width of the gain line and/or the location of its maximum. Finally, as in any resonator, temperature variations are of concern. Depending on the cavity's free spectral range (and this point is more crucial for longer devices), the actual position of the modes close to the gain peak may change during the transient evolution (or even during operation). The predictions of this model indicate that the laser may pass from one situation which can be correctly modeled with an even number of modes to one where an odd number of modes may be more appropriate (passing from all intermediate configurations). Thus, we may have to expect properties which correspond to some kind of *average* over the two extreme configurations we have chosen to examine.

VI. SUMMARY AND CONCLUSIONS

We have numerically investigated the dynamics of a multimode semiconductor laser in response to a sudden turn-on by a switch of a parameter (pump). The model consists of $(M + 1)$ ordinary differential equations that represent the M modal intensities, with coupling occurring through the population inversion (i.e., the carrier density).

We have first numerically shown, using a large number of modes ($M = 113$), that the two global variables (total intensity and population inversion) reach their respective steady state values in a time much shorter than the one necessary to attain a global steady state, while the individual modal intensities continue to evolve over a much longer time scale, internally redistributing their energy to satisfy the constraint of constant output. The numerics show that the mode with the highest gain is the slowest to reach steady state, over times which are approximately two orders of magnitude longer than those necessary to reach constant output intensity.

With the help of a simplified analysis, we have shown the existence of one master mode, the closest one to line center, which governs all the dynamical evolution of the modal content, and thus of the optical emission spectrum, toward its final state. The hidden time evolution (i.e., the energy redistribution among lasing modes) presents potential

difficulties in obtaining meaningful predictions, particularly for the spectral content.

Since it has already been proven that the shape of the gain line has only a minor influence on the quantitative aspects of the predictions [30], we can confidently assume that our considerations hold beyond the specific aspects of the semiconductor laser model considered. Indeed, the existence of a master mode, and the consequent slow evolution of the optical spectrum, holds true for all those lasers whose multi-longitudinal-mode operation can be described by intensity-coupled ODEs since it is the structure of the coupling which determines the dynamics, rather than the details of the model. It is therefore reasonable to expect that our results will apply, at least in part, to all class B lasers.

ACKNOWLEDGMENTS

We are grateful to S. Balle, M. Brambilla, C. R. Mirasso, M. San Miguel, and J. R. Tredicce for helpful discussions.

APPENDIX

The model used in this paper [13] has been chosen because of its favorable comparison with experimental results and because of the fact that the model's parameters have been determined through this comparison. The model equations are [13]

$$\frac{dI_j(t)}{dt} = \left[\Gamma G_j(N) - \frac{1}{\tau_p}\right] I_j + \beta_j B N(N+P_0), \quad \text{(A1a)}$$

$$\frac{dN(t)}{dt} = \frac{J}{q} - R(N) - \sum_j \Gamma G_j(N) I_j, \quad \text{(A1b)}$$

where $N(t)$ is the number of carriers as a function of time, $I_j(t)$ is the number of photons in the jth longitudinal mode of the e.m. field, J is the current injected into the active region, q is the electron charge, $R(N)$ is the incoherent recombination term (including radiative and nonradiative recombination) which represents the global loss terms for the carrier number (i.e., the population inversion in the usual laser language), Γ is the optical confinement factor, and τ_p is the photon lifetime in the cavity, defined by

$$\tau_p = \frac{n_g}{c\left(\alpha_0 + \frac{1}{2L}\ln\frac{1}{R_1 R_2}\right)}, \quad \text{(A2)}$$

with n_g being the group refractive index, c being the speed of light in vacuum, α_0 being the intrinsic attenuation coefficient, L being the geometric length of the laser cavity, and R_1 and R_2 being the (intensity) reflectivity coefficients for the two laser end faces.

The coefficient β_j is the fraction of spontaneous emission coupled into the jth lasing mode as defined in [13]. For convenience, we here use the index k with the following correspondence $\{k = k_{\min},(k_{\min}+1),\ldots \leftrightarrow j = 1,2,\ldots\}$:

$$\beta_k = \frac{\beta_0}{1 + f_k(\Delta\lambda_D, \Delta\lambda_s)}, \quad \text{(A3)}$$

$$f_k(\Delta\lambda_D,\Delta\lambda_s) = \begin{cases} \left[k\frac{2\Delta\lambda_D}{\Delta\lambda_s}\right]^2 & -\frac{M-1}{2} \leqslant k \leqslant \frac{M-1}{2}, \quad M \text{ odd} \\ \left[\left(k+\frac{1}{2}\right)\frac{2\Delta\lambda_D}{\Delta\lambda_s}\right]^2 & -\frac{M}{2} \leqslant k \leqslant \frac{M}{2}-1, \quad M \text{ even} \end{cases} \quad \text{(A4)}$$

where $\Delta\lambda_D$ represents the mode spacing:

$$\Delta\lambda_D = \frac{\lambda_p^2}{2n_g L}, \quad \text{(A5)}$$

with λ_p being the wavelength at the peak of the gain curve, $\Delta\lambda_s$ being the wavelength interval denoting the FWHM of the spontaneous emission, and β_0 being the maximum value of the spontaneous emission coefficient, defined by

$$\beta_0 = \frac{\lambda_p^4}{8\pi^2 n_g n_r^2 \Delta\lambda_s V_{\text{act}}}, \quad \text{(A6)}$$

with n_r being the index of refraction and V_{act} being the active laser volume. B is the band-to-band recombination coefficient, P_0 is the intrinsic hole number in the absence of injected current, and $G_j(N)$ is the optical gain for the jth lasing mode and is also a function of carrier number and wavelength.

$R(N)$ and $G(N)$, defined in [13], are explicitly given by

$$R(N) = AN + BN(N+P_0) + CN(N+P_0)^2, \quad \text{(A7)}$$

$$G_j(N) = g_p(N-N_0)(1-\epsilon I_t) \times \left[1 - 2\left(\frac{\lambda_j - \lambda_p}{\Delta\lambda_G}\right)^2\right], \quad \text{(A8)}$$

where A describes recombination processes via traps and surface states, B is the band-to-band recombination coefficient, and C is the Auger recombination constant. For the gain function $G(N)$, g_p is the gain peak value, N_0 is the carrier number at transparency, λ_j is the wavelength of the jth laser mode, λ_p is the wavelength of the gain peak, $\Delta\lambda_G$

TABLE III. Values of all parameters used for the simulation of the model equations of Ref. [13].

Parameter	Value	Parameter	Value
P_0	1.5×10^7	A	$10^8\ \text{s}^{-1}$
Γ	0.3	B	$2.788\ \text{s}^{-1}$
ϵ	9.6×10^{-8}	C	$7.3 \times 10^{-9}\ \text{s}^{-1}$
N_0	7.8×10^7	g_p	$2.628 \times 10^4\ \text{s}^{-1}$
n_g	4.0	λ_p	$1.3\ \mu\text{m}$
n_r	3.54	L	$350\ \mu\text{m}$
R_1, R_2	0.3	α_0	$30\ \text{cm}^{-1}$
q	1.6×10^{-19} C	V_{act}	$5.2 \times 10^{-11}\ \text{cm}^3$
$\Delta\lambda_s$	80 nm	$\Delta\lambda_G$	45 nm

is the FWHM wavelength of the gain curve, I_t is the total number of photons present in all the modes, and ϵ is the gain compression factor (taking into account gain saturation effects). All parameter values are given in Table III. In this paper we only consider the deterministic laser response and therefore do not add noise to the model.

[1] P. A. Khandokhin, P. Mandel, I. V. Koryukin, B. A. Nguyen, and Y. a. I. Khanin, Phys. Lett. A **235**, 248 (1997).

[2] G. Kozyreff and P. Mandel, Phys. Rev. A **58**, 4946 (1998).

[3] I. V. Koryukin and P. Mandel, Phys. Rev. A **70**, 053819 (2004).

[4] K. Otsuka, P. Mandel, S. Bielawski, D. Derozier, and P. Glorieux, Phys. Rev. A **46**, 1692 (1992).

[5] B. Peters, J. Hünkemeier, V. M. Baev, and Ya. I. Khanin, Phys. Rev. A **64**, 023816 (2001).

[6] P. Mandel, E. A. Viktorov, C. Masoller, and M. S. Torre, Physica A **327**, 129 (2003).

[7] A. M. Yacomotti, L. Furfaro, X. Hachair, F. Pedaci, M. Giudici, J. R. Tredicce, J. Javaloyes, S. Balle, E. A. Viktorov, and P. Mandel, Phys. Rev. A **69**, 053816 (2004).

[8] Y. Tanguy, J. Houlihan, G. Huyet, E. A. Viktorov, and P. Mandel, Phys. Rev. Lett. **96**, 053902 (2006).

[9] S. Osborne, A. Amann, K. Buckley, G. Ryan, S. P. Hegarty, G. Huyet, and S. OBrien, Phys. Rev. A **79**, 023834 (2009).

[10] M. Peil, I. Fischer, and W. Elsäßer, Phys. Rev. A **73**, 023805 (2006).

[11] G. Huyet, J. K. White, A. J. Kent, S. P. Hegarty, J. V. Moloney, and J. G. McInerney, Phys. Rev. A **60**, 1534 (1999).

[12] X. Zhang, H. Ye, and Z. Song, Chin. Opt. Lett.**6**, 120 (2008).

[13] D. M. Byrne, J. Lightwave Technol. **10**, 1086 (1992).

[14] L. M. Narducci and N. B. Abraham *Laser Physics and Laser Instabilities* (World Scientific, Singapore, 1988).

[15] J. R. Tredicce, F. T. Arecchi, G. L. Lippi, and G. P. Puccioni, J. Opt. Soc. Am. B **2**, 173 (1985).

[16] In a single-mode, class B laser analysis, this frequency would be $\propto \sqrt{\gamma_\parallel K}$, with $\gamma_\parallel$ and K being relaxation rates for the population and for the intracavity field, respectively [15].

[17] Cf. Chapter 7 of [18].

[18] P. Mandel, *Theoretical Problems in Cavity Nonlinear Optics* (Cambridge University Press, Cambridge, 1997).

[19] J. M. T. Thompson and H. B. Stewart, *Nonlinear Dynamics and Chaos* (Wiley, New York, 1986).

[20] G. L. Lippi, S. Barland, N. Dokhane, F. Monsieur, P. A. Porta, H. Grassi, and L. M. Hoffer, J. Opt. B **2**, 375 (2000).

[21] D. Marcuse and T. P. Lee, IEEE J. Quantum Electron. **19**, 1397 (1983).

[22] N. Dokhane and G. L. Lippi, Appl. Phys. Lett. **78**, 3938 (2001).

[23] The numerics show that the condition $\frac{dN}{dt}_{t=\bar{t}} = 0$ is only approximate, but the relative deviation is at most $\frac{\Delta N}{N} \simeq 10^{-5}$. Thus we can consider our analysis to hold quite well.

[24] Table I shows that the actual values of the prefactor for I_j are negative. We have put the sign explicitly in Eq. (7) and therefore take $a_j > 0$ for all values of j.

[25] The control of the dynamics by the slowest mode is a feature common to all dynamical systems close to a bifurcation (or a "phase transition"). see, e.g., [25] for the so-called slaving dynamics or [17] for time scale dynamics near a bifurcation point.

[26] H. Haken, *Synergetics: An Introduction* (Springer, Berlin, 1978).

[27] S. Balle, Opt. Commun. **119**, 227 (1995).

[28] S. Balle, Phys. Rev. A **57**, 1304 (1998).

[29] W. W. Chow and S. W. Koch, *Semiconductor-Laser Fundamentals* (Springer, Berlin, 1999).

[30] N. Dokhane, Ph.D. thesis, Université de Nice-Sophia Antipolis, 2000.